
Chapter 1

Microfluidics and fluorescence microscopy for cellular metabolic cycles

To reconcile the evidence about the characteristics of the yeast metabolic cycle (YMC) from single-cell and chemostat experiments, I sought to use a single-cell experimental platform to address whether cellular metabolic cycles confirm chemostat-based studies.

Few published studies have investigated the YMC in cells isolated from each other. Most studies instead have examined the YMC from a population of cells in a chemostat. However, such chemostat-based studies are unable to account for cell-to-cell heterogeneity. Furthermore, in such conditions, cell density and environmental conditions are far removed from the natural habitat of budding yeast.

In this chapter, I use single-cell microfluidics to physically separate budding yeast cells. In these experiments, I use fluorescence microscopy to monitor the yeast metabolic cycle and the cell division cycle.

Specifically, I aim to evaluate these hypotheses:

1. Yeast cells independently generate yeast metabolic cycles. Each cell generates the metabolic cycle autonomously of other cellular oscillators, but the metabolic cycle can phase-lock the cell division cycle.
2. The yeast metabolic cycle is retained in different nutrient and genetic perturbations, but characteristics of the cycle change in response.
3. Flavin autofluorescence of single yeast cells recapitulate oscillations in dissolved oxygen in the chemostat. If there are discrepancies between these two manifestations of the yeast metabolic cycle, cell-to-cell heterogeneity should explain the discrepancies. **synchrony in the chemostat?**

In this chapter, I show that metabolic cycles are generated autonomously and are coupled to the cell division cycle in permissive conditions, confirming previous single-cell studies. To decouple the metabolic and cell division oscillators, confirming that the metabolic oscillator is independently and autonomously generated, I used fast nutrient switching to induce starvation. I further show that the metabolic cycle is robust across nutrient and genetic perturbations, but with

citations changes to their oscillatory parameters. Finally, to address whether single-cell metabolic cycles confirm findings from chemostat-based ~~experimental~~ studies, I emulated situations known to affect dissolved-oxygen traces. These situations include potassium deficiency and deletions of genes with roles in metabolism and biological timekeeping.

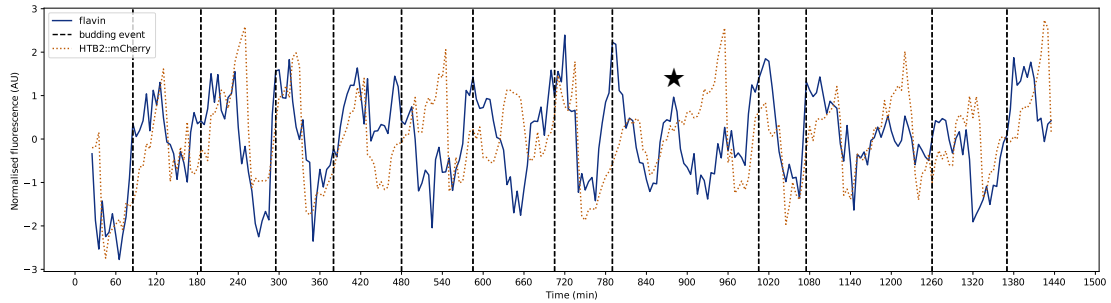


Figure 1.1: Flavin fluorescence (blue, solid lines) and histone 2B (orange, dotted lines) levels in a single, representative FY4 HTB2::mCherry cell grown in 20 g L^{-1} glucose. Vertical lines (black, dashed) indicate budding events. Star (*) indicates a flavin oscillation without a corresponding cell division cycle.

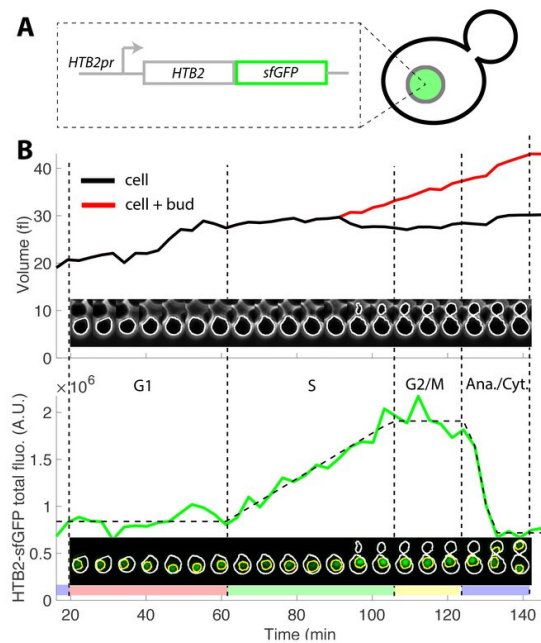


Figure 1.2: (A) Engineering a fluorescent protein cassette fused to *HTB2* (B) allows the identification of phases of the cell division cycle through monitoring changes in fluorescence of the fluorescent protein. Adapted from Garmendia-Torres et al. (2018).

1.1 Coupled oscillations in permissive conditions

To show that metabolic cycles are generated autonomously and are coupled to the cell division cycle, I replicated the single-cell flavin oscillations observed by Baumgartner et al. (2018). Replicating results from a previous flavin-based microfluidics study is important to confirm that my use of ALCATRAS (Crane et al., 2014) monitored the yeast metabolic cycle, especially given that the microfluidics set-up differed from previous studies (Papagiannakis et al., 2017; Baumgartner et al., 2018).

Fig. 1.1 shows that oscillations in flavin fluorescence peak when a bud forms in G₂/M, as evidenced by prototrophic FY4 HTB2::mCherry cells grown in minimal medium supplemented with 20 g L⁻¹ glucose. The HTB2::mCherry insertion allows monitoring phases of the cell division cycle through quantifying over time the intensity of the fluorescence of the inserted protein (Fig. 1.2), while also allowing monitoring flavin fluorescence by avoiding the overlap of flavin and GFP emission spectra.

Fig. 1.1 also shows that in some cases, a metabolic oscillation occurred without cell division cycle progression or bud formation. Such cases, also revealed by Papagiannakis et al. (2017) via cycles of NAD(P)H fluorescence, confirmed that the metabolic cycle is generated autonomously from the cell division cycle.

As observed, oxidation of flavin upon budding was expected for these reasons:

1. Flavin fluorescence peaks (becomes most oxidised) and NAD(P)H fluorescence peaks (becomes most reduced) at the same time in chemostat cultures (Murray et al., 2011).
2. NAD(P)H is in the reduced form when buds form (Papagiannakis et al., 2017).

3. The flavoprotein lipoamide dehydrogenase is in redox equilibrium with what is the gene name?
NAD(P)H (Siano and Mutharasan, 1989).

To quantify the period of the oscillators, I combined time series analysis methods. Fig. 1.3 shows that flavin fluorescence oscillated at a period of approximately 90 min, based on the mean Fourier spectrum and median autocorrelation function. Figs. 1.3b and 1.3d additionally show that the cell division cycle proceeded at the same period, as evidenced by the autocorrelation function of mCherry. The duration of the cell division cycles agrees with previously reported values (Herskowitz, 1988).

To visualise the relationship between the metabolic cycle and the cell division cycle, Fig. 1.4 shows that budding events synchronise with peaks in fluorescence and that the cell division cycle varies between cells, with most just under 2 h, agreeing with Fig. 1.3b (inset). The oscillatory shape of the median flavin fluorescence time series when aligned to the first budding event (Fig. 1.4b) further confirms the synchrony between the metabolic cycle and budding events.

Finally, to quantify the relationship between the metabolic cycle and the cell division cycle, I computed the cross-correlation function between the flavin and mCherry signals across the population (Fig. 1.4c). This function shows that the mCherry signal peaks are, on average, shifted by 5 min relative to the flavin signals, thus demonstrating the coincidence between peaks of flavin oscillations and mitosis.

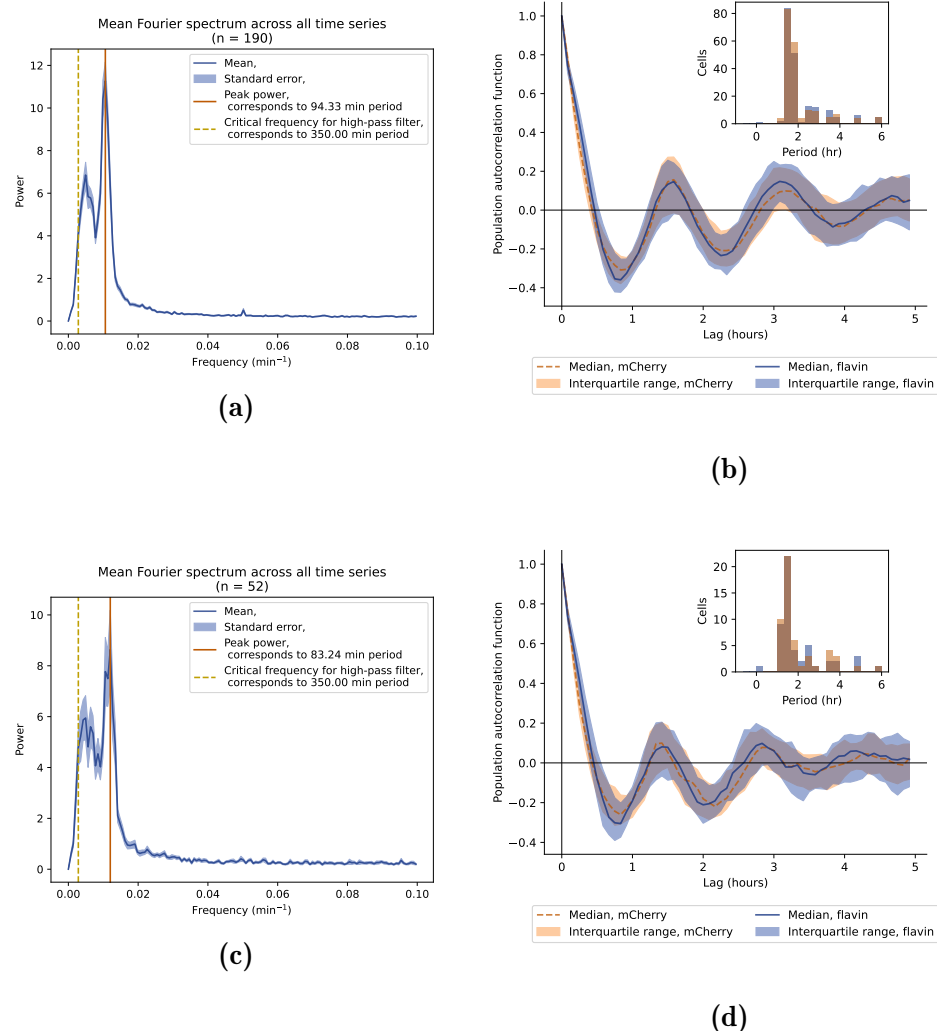


Figure 1.3: (1.3a, 1.3c) Mean Fourier spectrum of flavin fluorescence time series across cells. (1.3b, 1.3d) Median autocorrelation functions of flavin fluorescence (blue) and histone 2B levels (orange) time series, along with (*insets*) the periods of each oscillator across cells as determined by the frequency with the greatest power in each signal's Fourier spectrum. Data are from FY4 HTB2::mCherry cells under 20 g L^{-1} glucose; two experiment repeats shown.

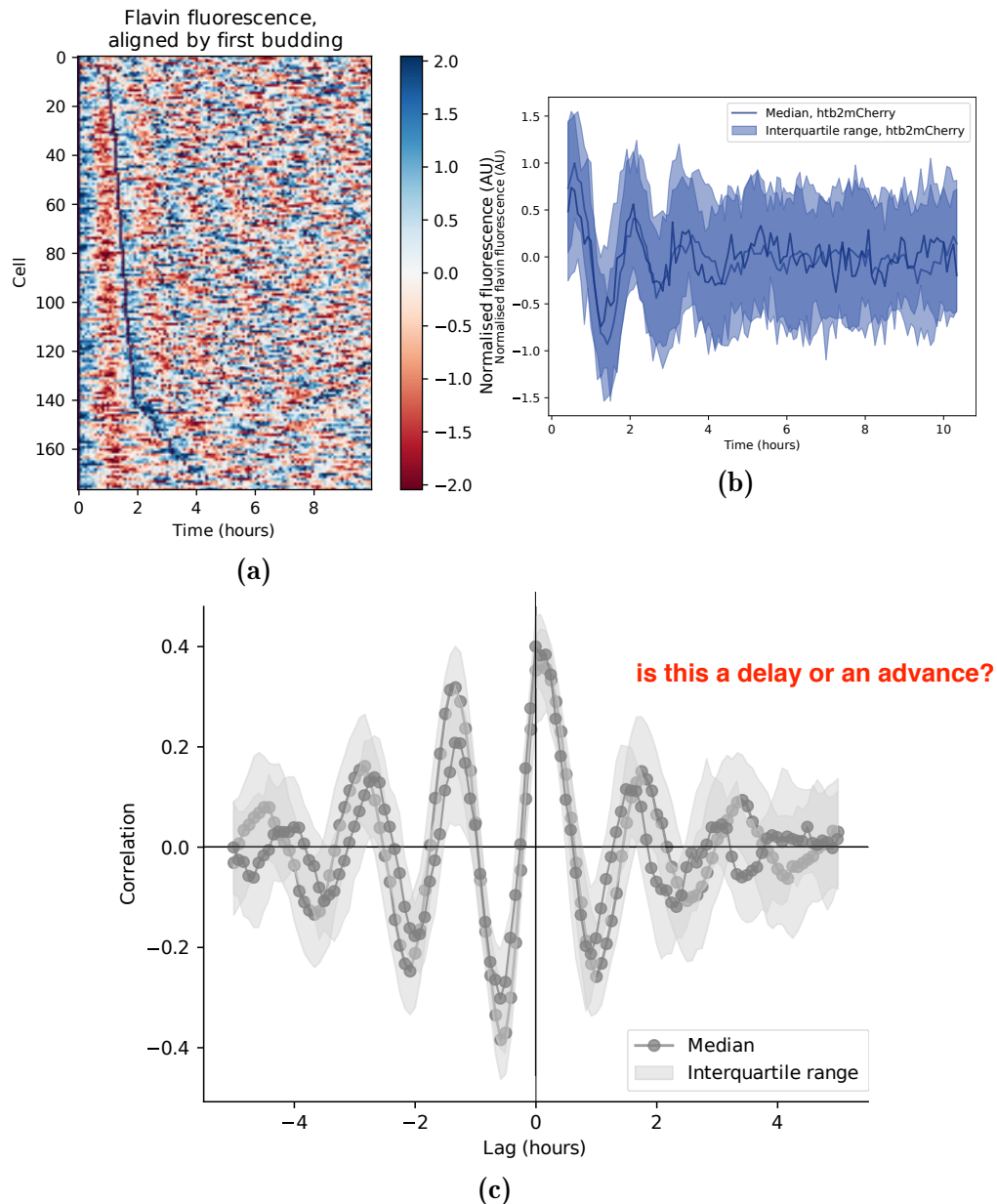


Figure 1.4: (1.4a) Heatmap showing the flavin fluorescence (pixels on a red-blue scale) and budding events (black pixels) of each cell over time. Signals are aligned by the first budding event. (1.4b) Median flavin fluorescence signal across cells, aligned to first budding event (two repeats: $n_1 = 361$, $n_2 = 144$). (1.4c) Median cross-correlation function between flavin and histone 2B signals (two repeats: $n_1 = 392$, $n_2 = 170$). Data are from FY4 HTB2::mCherry cells in 20 g L^{-1} glucose.

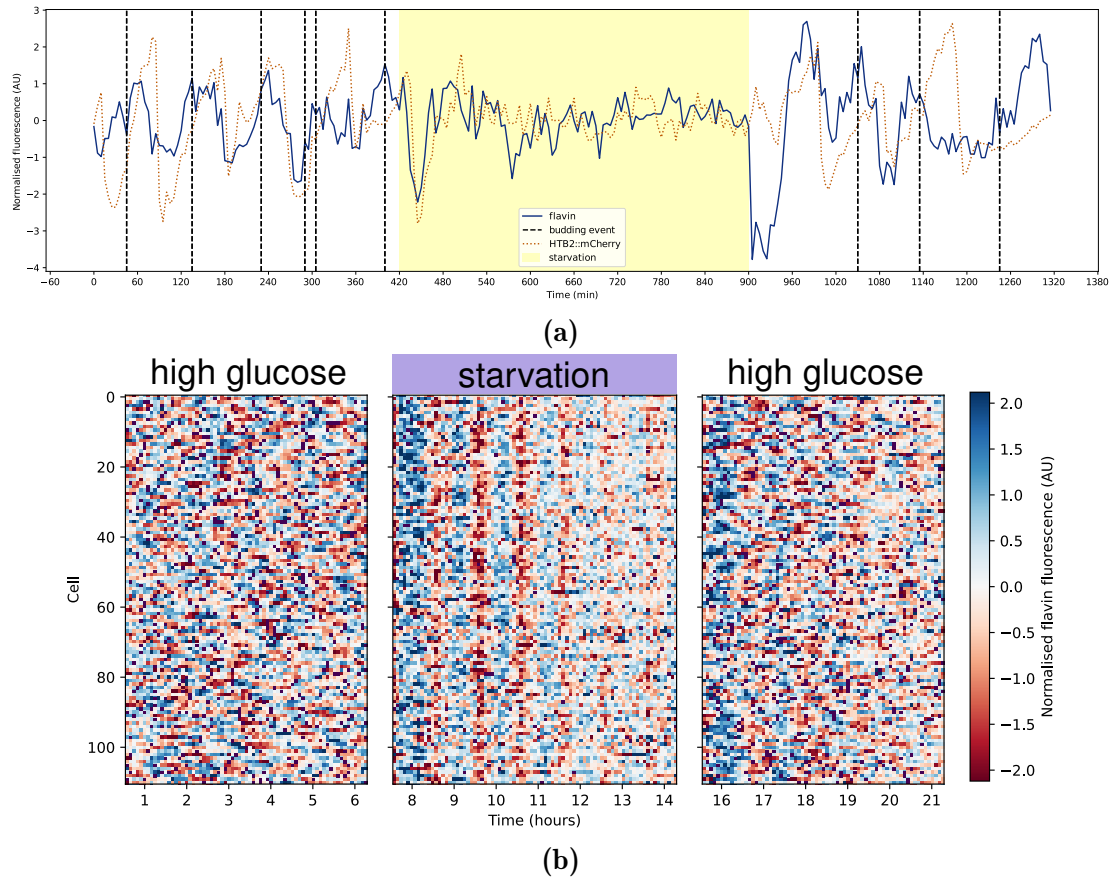


Figure 1.5: **(1.5a)** Flavin fluorescence (blue, solid lines) and histone 2B (orange, dotted lines) levels in a single, representative FY4 HTB2::mCherry cell. Vertical lines (black, dashed) indicate budding events. Shading (yellow) indicates glucose starvation. **(1.5b)** Heatmap showing the flavin fluorescence (pixels on a red-blue scale) and budding events (black pixels) of each cell. Data are from FY4 and HTB2::mCherry cells, subject to 7.5 g L^{-1} glucose for 7 h before being abruptly switched to 0 g L^{-1} glucose for 8 h and then resumed to 7.5 g L^{-1} glucose for 7 h.

1.2 Decoupling between the metabolic and cell division cycles

To provide additional evidence that cells generate metabolic oscillations autonomously of the cell division cycle, I created a condition in which cells did not undergo cell division. Specifically, I did so by inducing starvation: I cultured FY4 and HTB2::mCherry cells in 7.5 g L^{-1} glucose for 7 h, switching them to 0 g L^{-1} glucose

**what's plotted? why
doesn't it recover
when glucose
returns?**

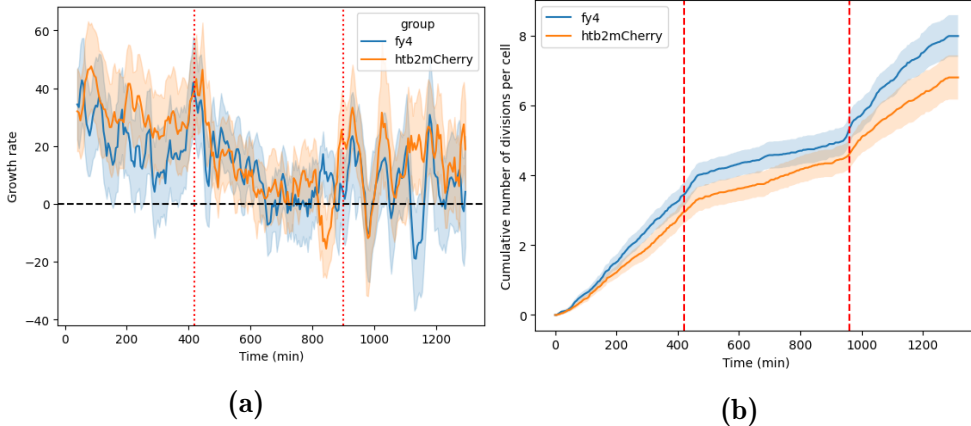


Figure 1.6: (1.6a) Mean growth rate (shading: 95% confidence intervals) and (1.6b) mean cumulative number of budding events per cell (shading: confidence intervals from bootstrapping, $n = 30$) of FY4 (blue) and HTB2::mCherry (orange) strains over time during the glucose-starvation experiment. Vertical lines (red) show changes in the nutrient medium.

for 8 h, and then resumed 7.5 g L^{-1} glucose for 7 h. This abrupt induction of starvation is similar to experiments described by Bagamery et al. (2020), which showed that a population of genetically identical budding yeast cells, upon glucose starvation, formed two subpopulations that had different cellular physiology.

Fig. 1.5 shows that when cells were in high glucose, metabolic oscillations were asynchronous, consistent with section 1.1, Papagiannakis et al. (2017), and Baumgartner et al. (2018). When cells grown in high glucose were abruptly starved of glucose, their flavin oscillations reset their phase. During starvation, these flavin oscillations continued, while growth rate dropped and budding events were sparse (Fig. 1.6).

The results show that metabolic oscillations can be generated when the cell division cycle is halted, providing strong evidence that the metabolic cycle is generated autonomously and independently of the cell division cycle. In addition, the results show that each cell can individually reset the phase of its metabolic cycle in response to abrupt changes in environmental conditions. Similar phe-

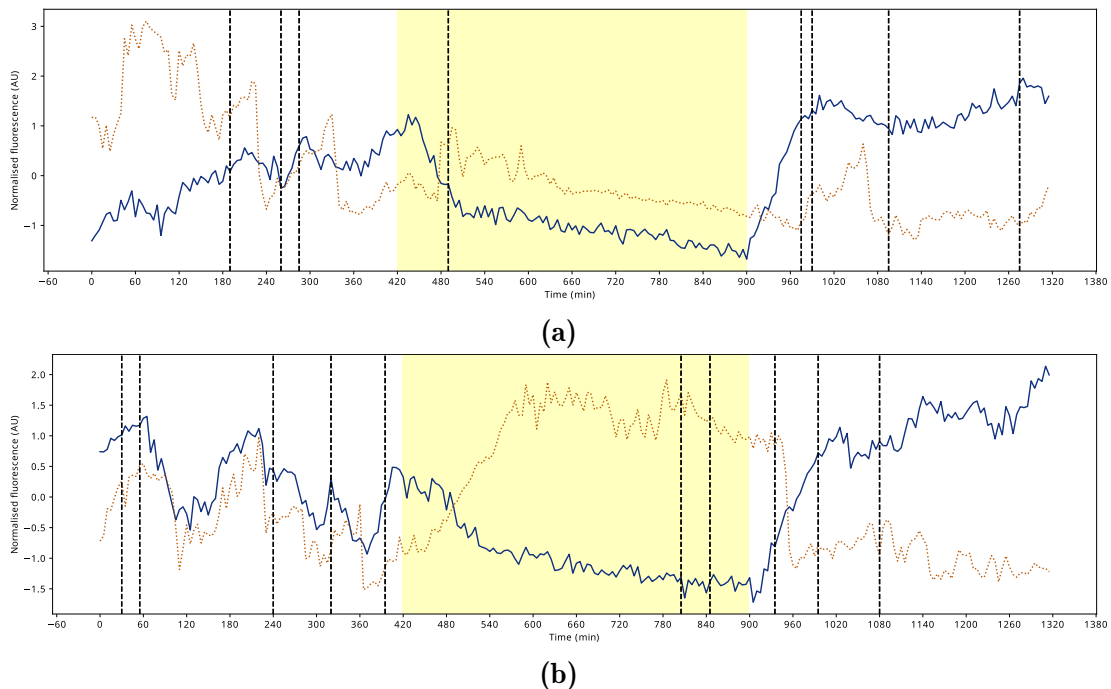


Figure 1.7: Flavin fluorescence (blue, solid lines) and histone 2B (orange, dotted lines) levels in two sample FY4 HTB2::mCherry cells in the glucose starvation experiment. Vertical lines (black, dashed) indicates budding events. Shading (yellow) indicate glucose starvation. **(1.7a)** is an example of a cell with a low intensity of mCherry during starvation, while **(1.7b)** is an example with a high intensity of mCherry. The flavin and mCherry time series were normalised to give a mean of 0 and standard deviation of 1 so that they can be plotted on the same vertical axes, but the high-pass Butterworth filter was not applied.

nomena have been observed upon bulk addition of carbon sources (Kuang et al., 2017; Krishna and Laxman, 2018). Importantly, the results suggest that diffusion of signalling chemicals between cells is not required for generation of metabolic cycles. Combined with results from the previous section, my results suggest that the metabolic cycle responds to external conditions and create windows of opportunity for initiating the cell division cycle, if conditions are favourable for growth.

**is there
memory of
the starvation
in the flavin
signal?**

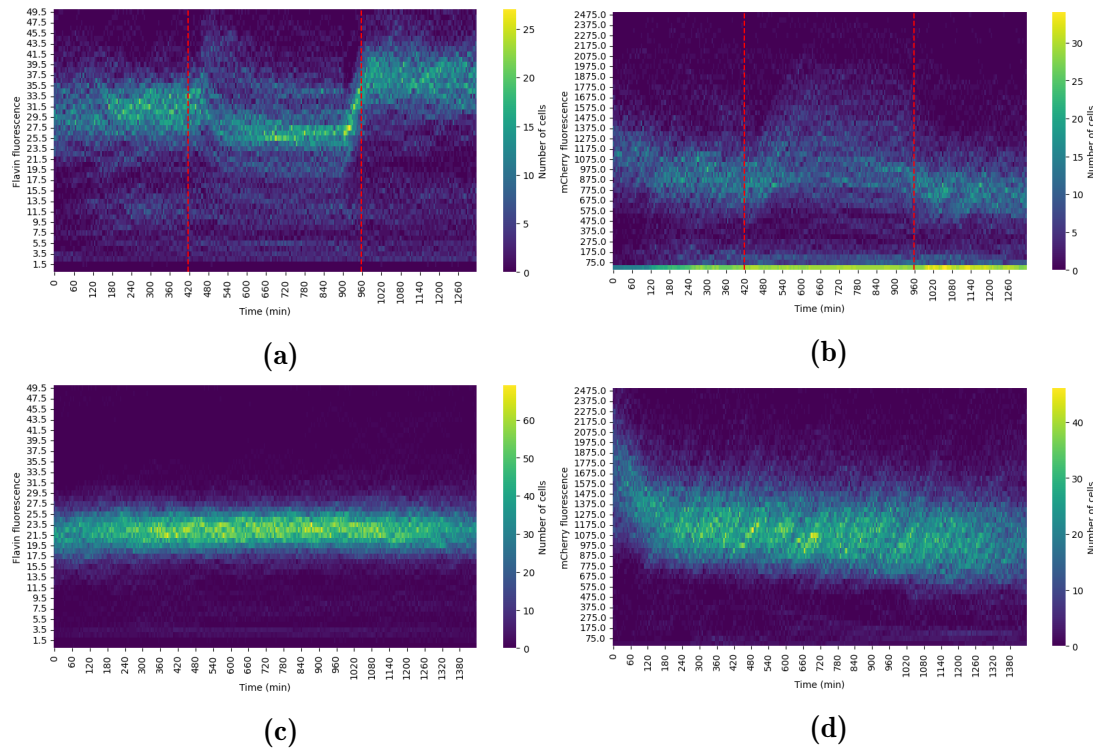


Figure 1.8: Distributions of (1.8a) flavin and (1.8b) mCherry fluorescence over time, for the glucose-starvation experiment. Vertical lines (red, dashed), indicate times of medium changes. As a control, distributions of (1.8c) flavin and (1.8d) mCherry fluorescence over time for the high glucose (20 g L^{-1}) experiment are also shown. Raw time series were used to calculate the distributions.

yeast has
short G2, it's
probably M
phase or at
least G2/M
phase

The model in which the metabolic cycle creates windows of opportunity for the cell division cycle implies that, upon starvation, cell division cycles progress to the next gap phase (G_1 or G_2) while the metabolic cycle continues. To test this implication, Fig. 1.7 shows that cells may remain in G_1 (Fig. 1.7a), as evidenced by low mCherry intensity, or in G_2 (Fig. 1.7b), as evidenced by high mCherry intensity. Extending this investigation across a population of cells, Fig. 1.8b shows that the distribution of mCherry intensity becomes broader during starvation before resuming to a distribution resembling the initial condition upon restoration of glucose. This observation can be explained by a larger proportion of cells in G_2 , giving high mCherry intensity, in contrast to the usually short time cells spend in G_2 relative to the rest of the cell division cycle (Fig. 1.2). In contrast, Fig. 1.8a suggests that during starvation, the distribution of flavin intensity became narrower. This observation can be explained by lower-amplitude oscillations during starvation, which was evidenced by a lower signal-to-noise ratio ($\bar{x}_{\text{before}} = 2.86$, $\bar{x}_{\text{starvation}} = 2.17$, $\bar{x}_{\text{after}} = 4.09$; Welch's t -test: starvation vs before $p = 0.009$, starvation vs after $p = 2.5 \times 10^{-12}$).

1.3 Metabolic cycles in different genetic backgrounds

To show that the metabolic cycle is robust, I monitored flavin autofluorescence signals from the auxotrophic BY4741 strain. Cells of this strain were grown in minimal medium supplemented with uracil and the amino acids required for this strain to grow, in addition to 10 g L^{-1} glucose as the carbon source. Showing that metabolic cycles occur in an auxotroph is important because it shows that many cellular aspects must be impaired for the cycle to disappear, thus suggesting that the metabolic cycle is an intrinsic property of budding yeast. Similar to FY4

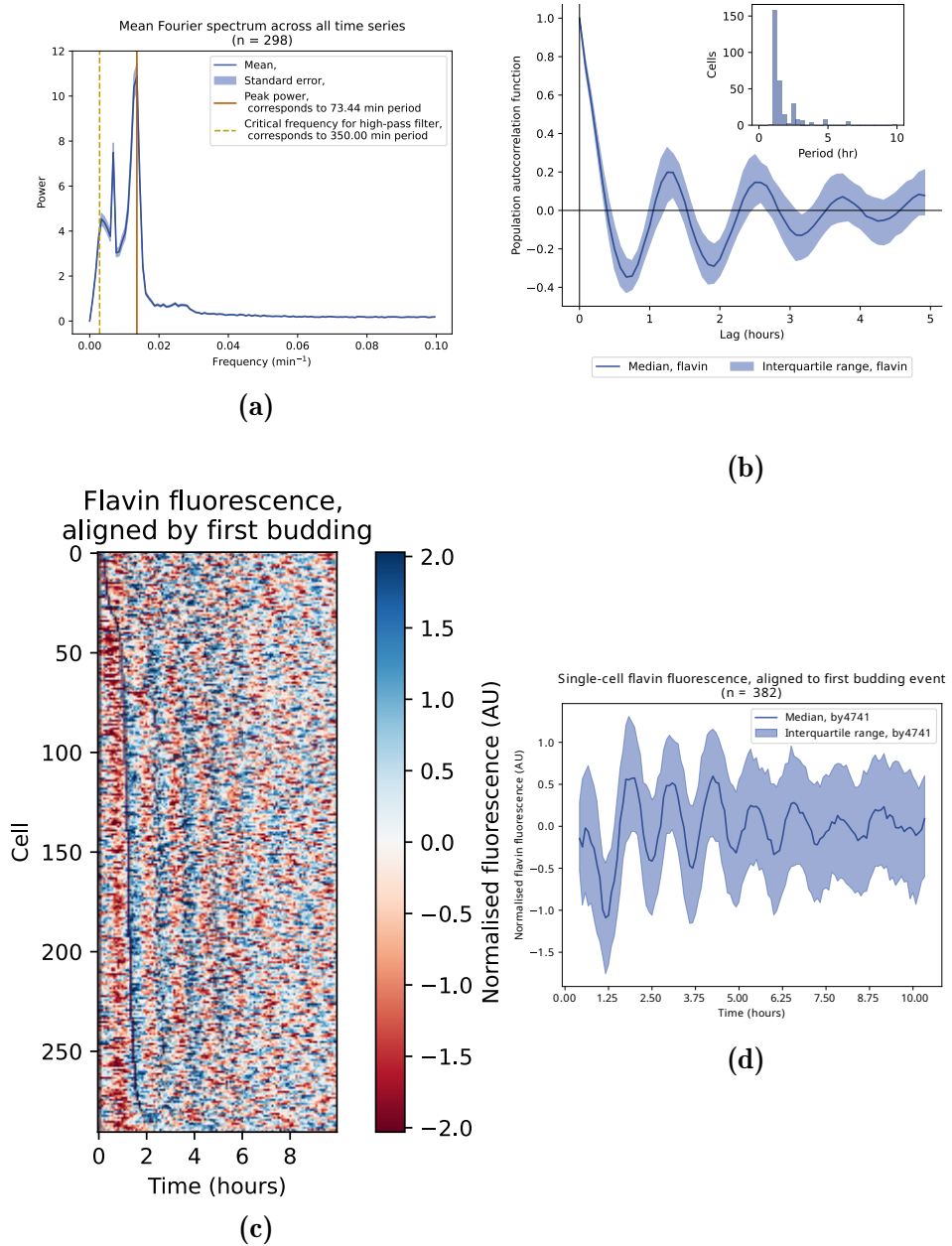


Figure 1.9: (1.9a) Mean Fourier spectrum of flavin fluorescence time series across cells. (1.9b) Median autocorrelation function of flavin fluorescence time series, along with (*inset*) the periods across cells as determined by the frequency with the greatest power in each signal's Fourier spectrum. (1.9c) Heatmap showing the flavin fluorescence (pixels on a red-blue scale) and budding events (black pixels) of each cell. Signals are aligned by the first budding event. (1.9d) Median flavin fluorescence signal across cells, aligned to first budding event. Data are from BY4741 cells in 10 g L^{-1} glucose.

HTB2::mCherry cells, BY4741 cells showed robust, consistent oscillations in flavin fluorescence that peak upon budding (figure 1.9), although metabolic cycles have a period of ≈ 75 min in this case. The shorter period may be explained by a lack of burden caused by a lack of an mCherry insertion, and by nutritional supplements.

FY4 and BY4741 both derive from the S288c background strain. To show that the metabolic cycle is generated from a budding yeast strain other than S288c background strains, I performed a similar experiment with the prototrophic CEN.PK strain grown in minimal medium. Showing that metabolic cycles additionally occur in a different genetic background is important to emphasise that the cycles

also the mitochondria are more stable (?) are intrinsic to budding yeast. CEN.PK is an important background to consider because it harbours genetic differences relative to S288c that results in physiological differences, including biotin prototrophy and malate metabolism (Nijkamp et al., 2012). Fig. 1.10 suggests that CEN.PK113-7D cells exhibited 90 min flavin oscillations that were synchronised with budding events, similar to FY4 cells, thus further confirming the robustness of the metabolic cycle across genetic backgrounds.

1.4 Metabolic cycles in different carbon sources

To show that the metabolic cycle responds to nutrient conditions and, accordingly, adjusts the cell's metabolism and cell division cycle, I cultured cells in pyruvate and in a growth-limiting glucose concentration. These experiments are important as they confirm conclusions about varying nutrient conditions made by Papagiannakis et al. (2017), but using flavin autofluorescence. Specifically, pyruvate provided an example of a non-fermentable carbon source to test whether

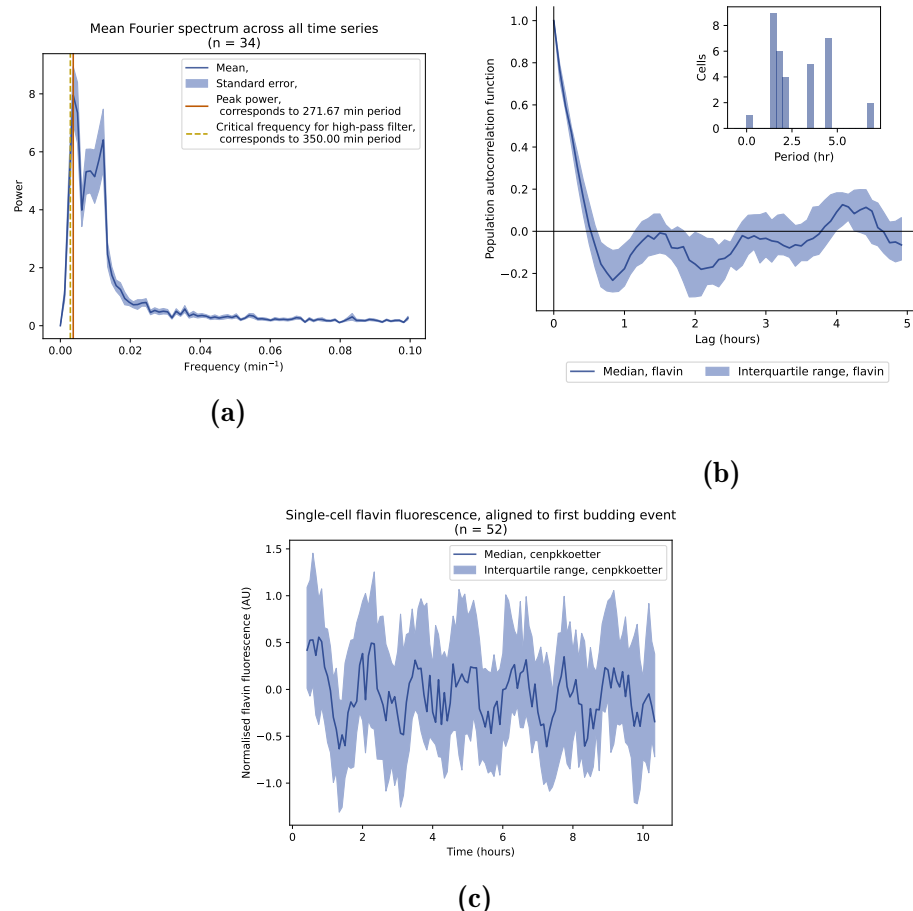


Figure 1.10: (1.10a) Mean Fourier spectrum of flavin fluorescence across cells. (1.10b) Median autocorrelation function of flavin fluorescence time series, along with (*inset*) the periods across cells as determined by the frequency with the greatest power in each signal's Fourier spectrum. (1.10c) Median flavin fluorescence signal across cells, aligned to first budding event. Data are from CEN.PK113-7D cells in 10 g L^{-1} glucose.

the switch from fermentative to respiratory metabolism affected the metabolic cycle. Additionally, a growth-limiting glucose concentration emulated low-glucose concentrations in a chemostat and was thus used to test whether long YMCs observed in such conditions can be replicated in a microfluidics platform.

Fig. 1.11 shows that FY4 HTB2::mCherry cells had longer metabolic cycles and cell division cycles (approximately 4 h) when grown in minimal media supplemented with 20 g L^{-1} pyruvate, compared to growth in high glucose. Furthermore, the synchrony between the two oscillators remained, but with a longer lag of the cell division cycle with respect to the metabolic cycle (Fig. 1.11c). Figure 1.11a shows that the longer cell division cycles were because of longer G₁ phases but unchanged S/M phases, as evidenced by the longer flat regions of the mCherry signal.

Fig. 1.12 shows that FY4 HTB2::mCherry cells had longer metabolic cycles when grown in minimal media supplemented with 10 mg L^{-1} glucose. Additionally, Fig. 1.13 shows that the growth rate and the rate of bud formation of cells on limiting glucose was lower than on high glucose (20 g L^{-1}). Furthermore, Fig. 1.14 shows that the amplitude of the flavin oscillations in this glucose-limiting condition was low relative to other conditions, as evidenced by the lower signal-to-noise ratios.

measurements of
Finally, Fig. 1.12b shows that the metabolic cycle and the cell division cycle lost synchrony in limiting glucose. This was evidenced by a 2.5 h average metabolic cycle, though not robust, but an absence of consistent oscillations in mCherry intensity. This decoupling can be explained by a lack of cell division cycle events.

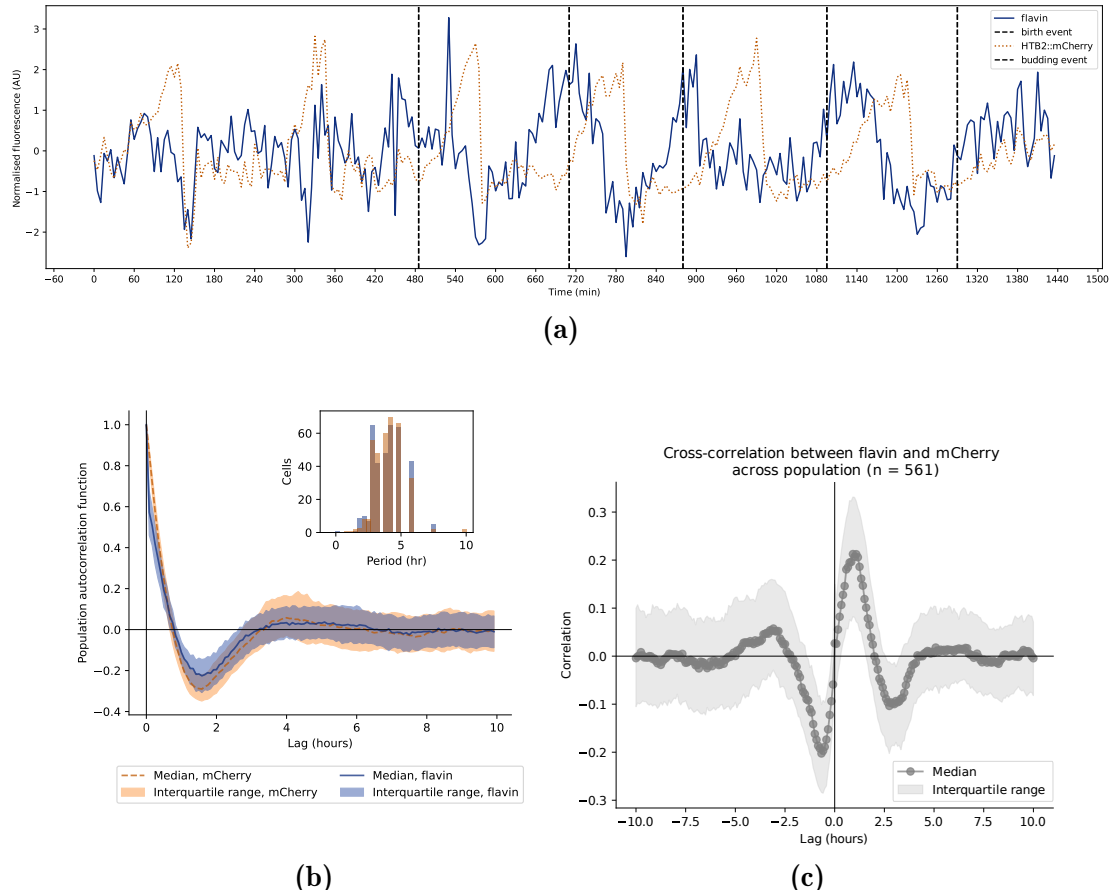
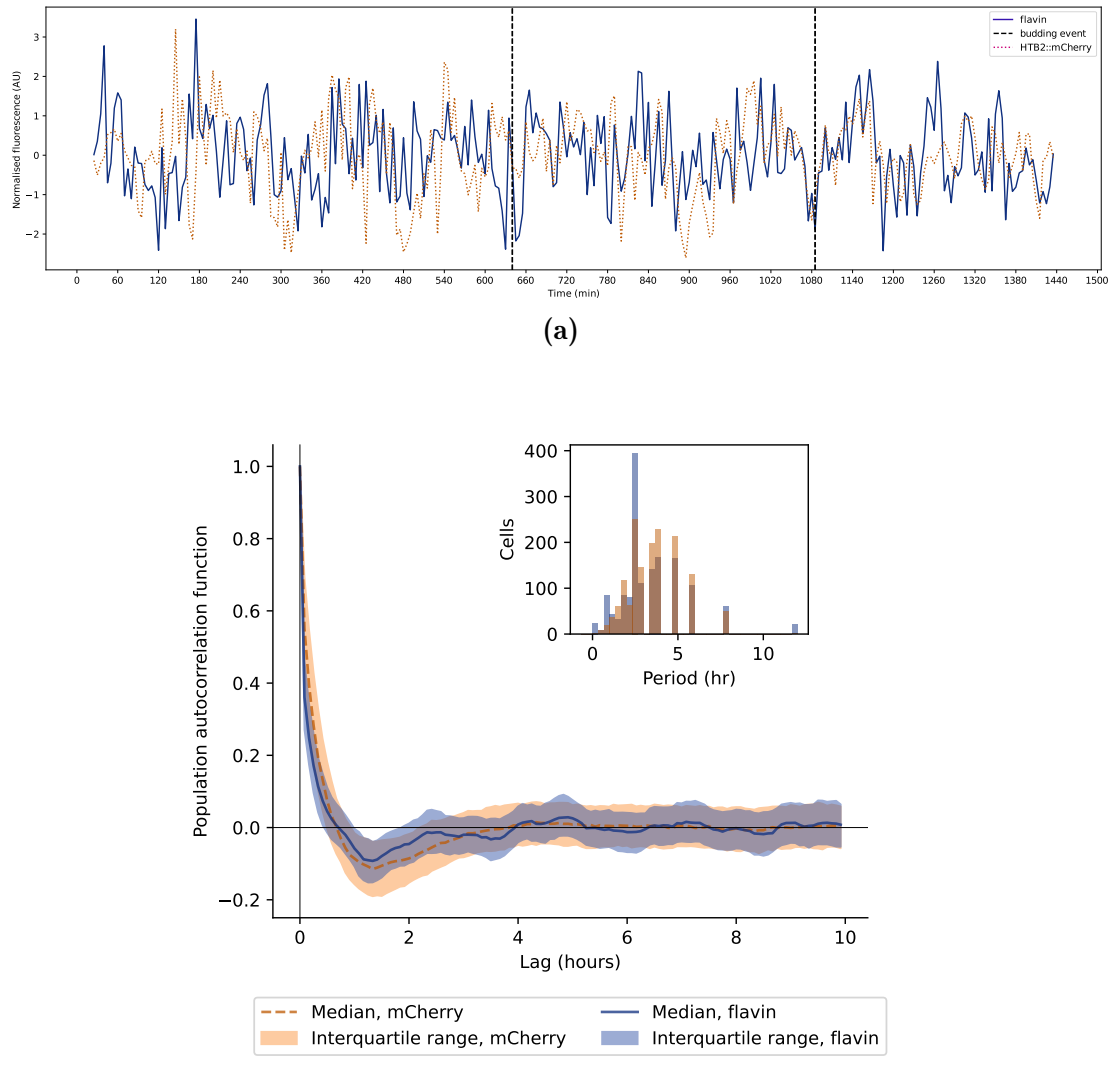


Figure 1.11: (1.11a) Flavin fluorescence (blue, solid lines) and histone 2B (orange, dotted lines) levels in a single, representative FY4 HTB2::mCherry cell grown in 20 g L^{-1} pyruvate. Vertical lines (black, dashed) indicate budding events. (1.11b) Median autocorrelation functions of flavin fluorescence (blue) and histone 2B levels (orange) time series, along with (*inset*) the periods of each oscillator across cells as determined by the frequency with the greatest power in each signal's Fourier spectrum. (1.11c) Median cross-correlation function between flavin and histone 2B signals. Data are from FY4 HTB2::mCherry cells in 20 g L^{-1} pyruvate.



keeping concs in g L⁻¹ would be clearer

Figure 1.12: (1.12a) Flavin fluorescence (blue, solid lines) and histone 2B (orange, dotted lines) levels in a single, representative FY4 HTB2::mCherry cell grown in 10 mg L⁻¹ glucose. Vertical lines (black, dashed) indicate budding events. (1.12b) Median autocorrelation functions of flavin fluorescence (blue) and histone 2B levels (orange) time series, along with (*inset*) the periods of each oscillator across cells as determined by the frequency with the greatest power in each signal's Fourier spectrum. Data are from FY4 HTB2::mCherry cells in 10 mg L⁻¹ glucose.

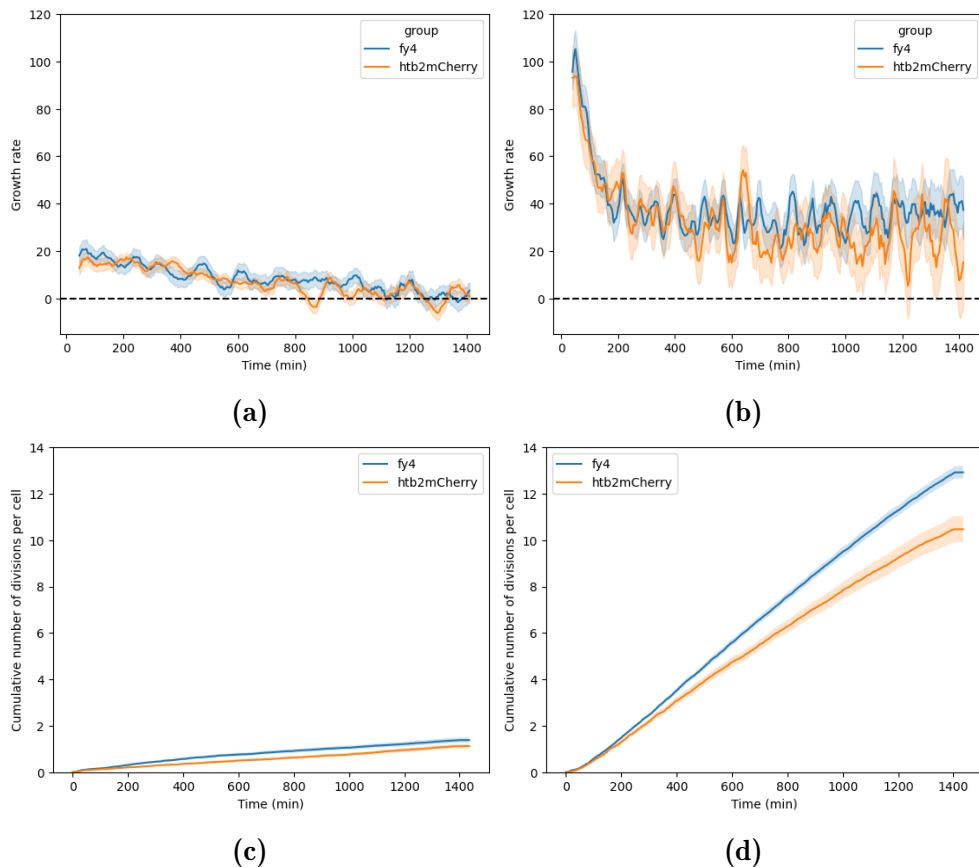


Figure 1.13: Mean growth rate of (shading: 95% confidence intervals) FY4 (blue) and HTB2::mCherry (orange) strains over time, for (1.13a) the glucose-limiting condition (10 mg L^{-1}) and (1.13b) the high glucose condition (20 g L^{-1}). Similarly, the mean cumulative number of budding events per cell (shading: confidence intervals from bootstrapping, $n = 30$), of the same strains for (1.13c) the glucose-limiting condition and (1.13d) the high glucose condition.

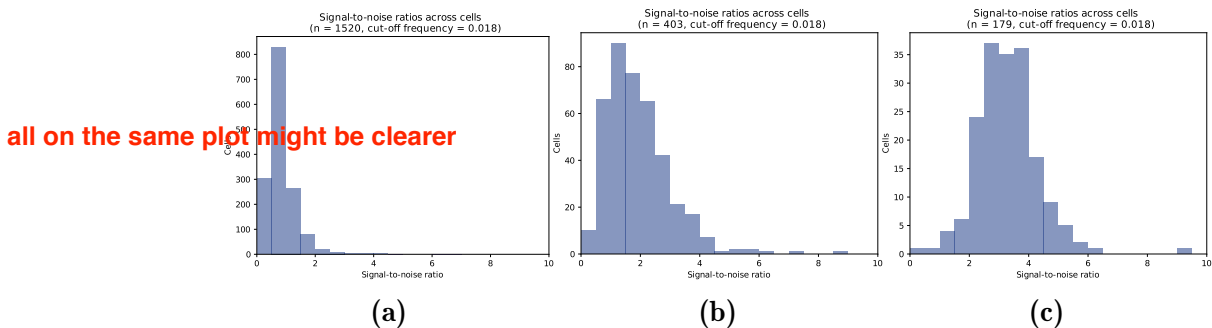


Figure 1.14: Distribution of signal-to-noise ratios of flavin signals from cells in (1.14a) 10 mg L^{-1} glucose, (1.14b) 20 g L^{-1} pyruvate, and (1.14c) 20 g L^{-1} glucose.

1.5 Metabolic cycles persist in potassium-deficient media

To address whether single-cell flavin traces from microfluidic experiments recapitulate dissolved-oxygen yeast metabolic cycles in chemostats, I replicated conditions of chemostat-based studies in which nutrient or genetic perturbations severely affected the metabolic cycle. These nutrient conditions included potassium deficiency and deletion strains included *zwf1Δ* and *tsa1Δ tsa2Δ*. Replicating conditions of chemostat-based studies is important in showing that the single-cell metabolic cycle and the chemostat metabolic cycle are the same cycle, or to prove otherwise. Chemostat experiments obscure the behaviour of individual cells, and single-cell microfluidics experiments can provide a bottom-up explanation of high-level observations of the metabolic cycle in the chemostat. Such single-cell experiments could address, for example, whether the cellular behaviour of the yeast metabolic cycle explains the changes in dissolved-oxygen oscillations.

To test whether potassium deficiency eliminates metabolic cycles, Fig. 1.15a shows that FY4 HTB2::mCherry cells retained synchronised metabolic cycles and cell division cycles when cells were abruptly switched from potassium-containing to potassium-deficient minimal medium (both media supplemented with 20 g L^{-1} as a carbon source). Such cycles were longer and were generated less reliably as in the normal growth medium (Fig. 1.15b). Furthermore, although the changes in the mean signal-to-noise ratio as the medium changed were significant (Fig. 1.16; $\bar{x}_{\text{before}} = 2.22$, $\bar{x}_{\text{deficient}} = 2.44$, $\bar{x}_{\text{after}} = 1.79$; Welch's *t*-test: deficient vs before $p = 0.015$, deficient vs after $p = 1.26 \times 10^{-12}$), the differences were more subtle than in the glucose-starvation experiment.

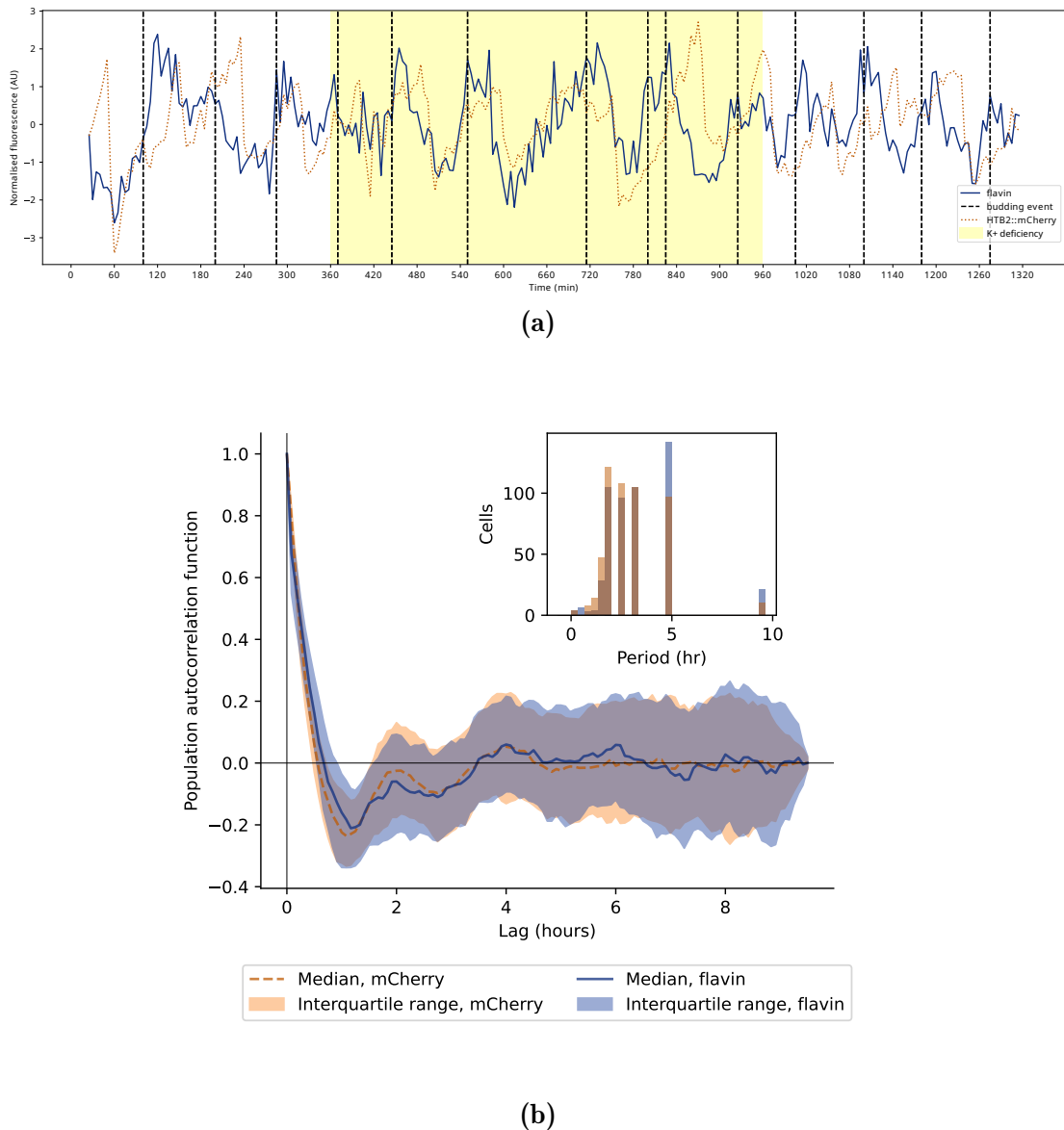


Figure 1.15: (1.15a) Flavin fluorescence (blue, solid lines) and histone 2B (orange, dotted lines) levels in a single, representative FY4 HTB2::mCherry cell. Vertical lines (black, dashed) indicate budding events. Shading (yellow) indicates the potassium-deficient period. (1.15b) Median autocorrelation functions of flavin fluorescence (blue) and histone 2B levels (orange) time series, along with (*inset*) the periods of each oscillator across cells as determined by the frequency with the greatest power in each signal's Fourier spectrum. Data are from FY4 and HTB2::mCherry cells; autocorrelation functions only used time points from the potassium-deficient condition (6 h to 16 h).

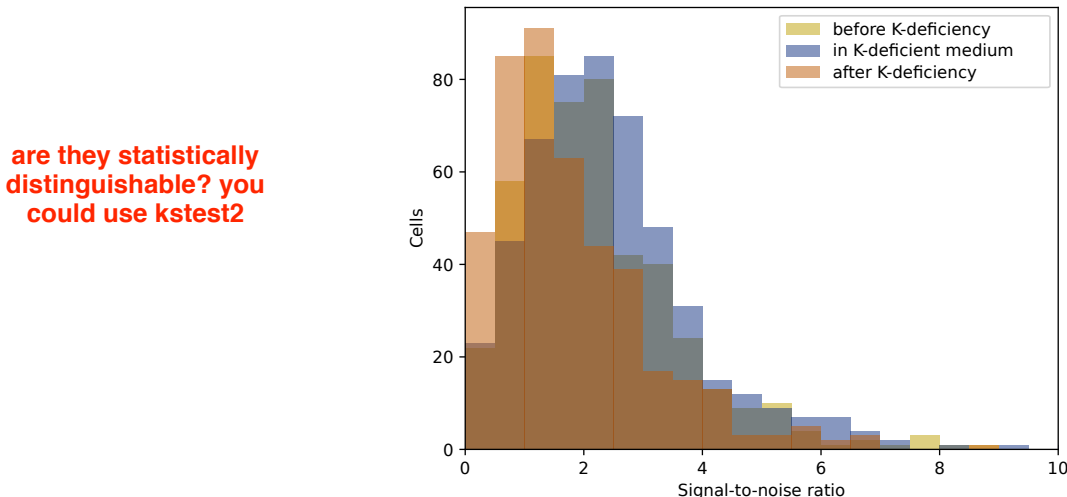


Figure 1.16: Distributions of signal-to-noise ratios of flavin signals from cells before, during, and after potassium-deficiency.

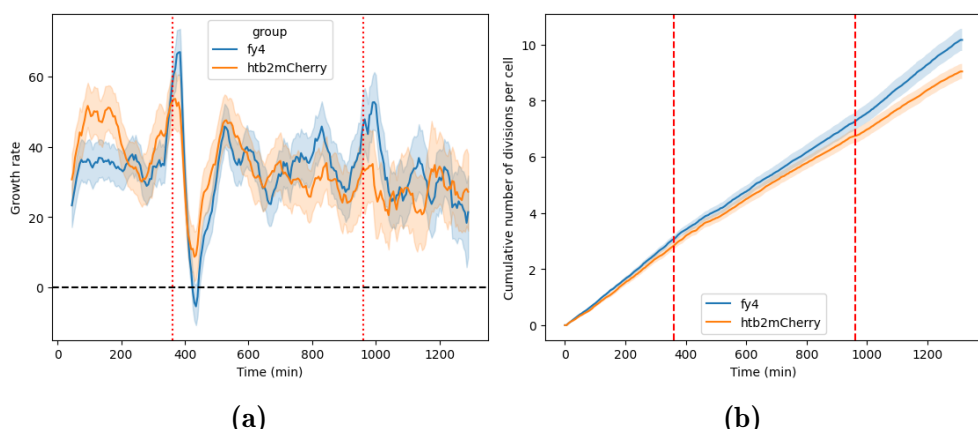


Figure 1.17: (1.17a) Mean growth rate (shading: 95% confidence intervals) and (1.17b) mean cumulative number of budding events per cell (shading: confidence intervals from bootstrapping, $n = 30$) of FY4 (blue) and HTB2::mCherry (orange) strains over time during the potassium-deficient experiment. Vertical lines (red) show changes in the nutrient medium.

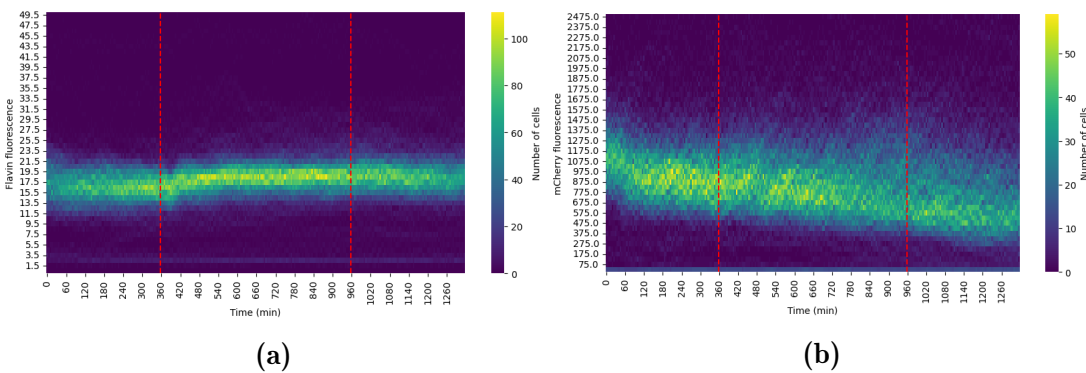


Figure 1.18: Distributions of (1.18a) flavin and (1.18b) mCherry fluorescence over time, for the potassium-deficient experiment. Vertical lines (red, dashed), indicate times of medium changes. Raw time series were used to calculate the distributions.

is there a time scale or number of cycles issue?
are we comparing at similar points?

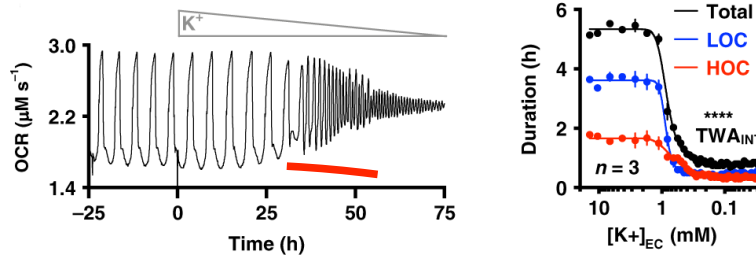


Figure 1.19: Decreasing extracellular potassium (K^+) concentration shortens, then under 1 mmol dm^{-3} , destroys metabolic oscillations in the chemostat. Adapted from O' Neill et al. (2020).

In addition, to test whether potassium deficiency affected cell growth and division, Fig. 1.17a shows that growth rates recovered soon after a sharp decrease upon the abrupt switch to the potassium-deficient medium. Fig. 1.17b further shows that the rate of budding was unaffected during potassium-deficiency, in contrast to a pause under glucose starvation (Fig. 1.6b). Finally, in contrast to glucose starvation, Fig. 1.18 suggests that potassium deficiency did not affect the time each cell spent in each phase of the metabolic and cell division cycles as they progressed through growth.

Results thus show that even though there was an initial response to potassium depletion, cells resumed growth, division, and generation of metabolic cycles soon after. My observations indicate that the metabolic cycle still occurs with a consistent amplitude, as evidenced by signal-to-noise ratios, in a drastically changed nutrient condition. This is in contrast to O' Neill et al. (2020), which suggested that, in chemostat cultures, as potassium in the nutrient medium is gradually replaced with sodium, the amplitude of dissolved-oxygen oscillations decreases until the oscillations disappear altogether (Fig. 1.19). However, my observations also warrant a model to reconcile the apparent differences between the chemostat and single-cell investigations.

move earlier in
this section. did
you try replacing
potassium with
sodium? sodium
is supposed to
be toxic.

1.6 Metabolic cycles in deletion strains

To continue the investigation of whether single-cell flavin-based metabolic cycles recapitulate dissolved-oxygen metabolic cycles, I investigated the *zwf1Δ* and *tsa1Δ tsa2Δ* deletion strains. The investigation of deletion strains is important as they can lead to mechanistic explanations of the YMC.

To investigate whether the *zwf1Δ* strain shows abolition of the metabolic cycle in single-cell microfluidics, I used a *zwf1Δ* strain with the BY4741 background. Chemostat-based studies have suggested that in the *zwf1Δ* strain, metabolic cycles are abolished but with little change in growth rate (Tu et al., 2007). Cells were pre-cultured in 20 g L⁻¹ pyruvate over 48 h and then cultured in 10 g L⁻¹ glucose in the microfluidic device because higher glucose concentrations disfavour growth in this strain. As the strain had an auxotrophic background, the required nutrient supplements were also added. Figure 1.20 shows that the *zwf1Δ* cells showed oscillations of approximately 3 h, but with low robustness and a wide

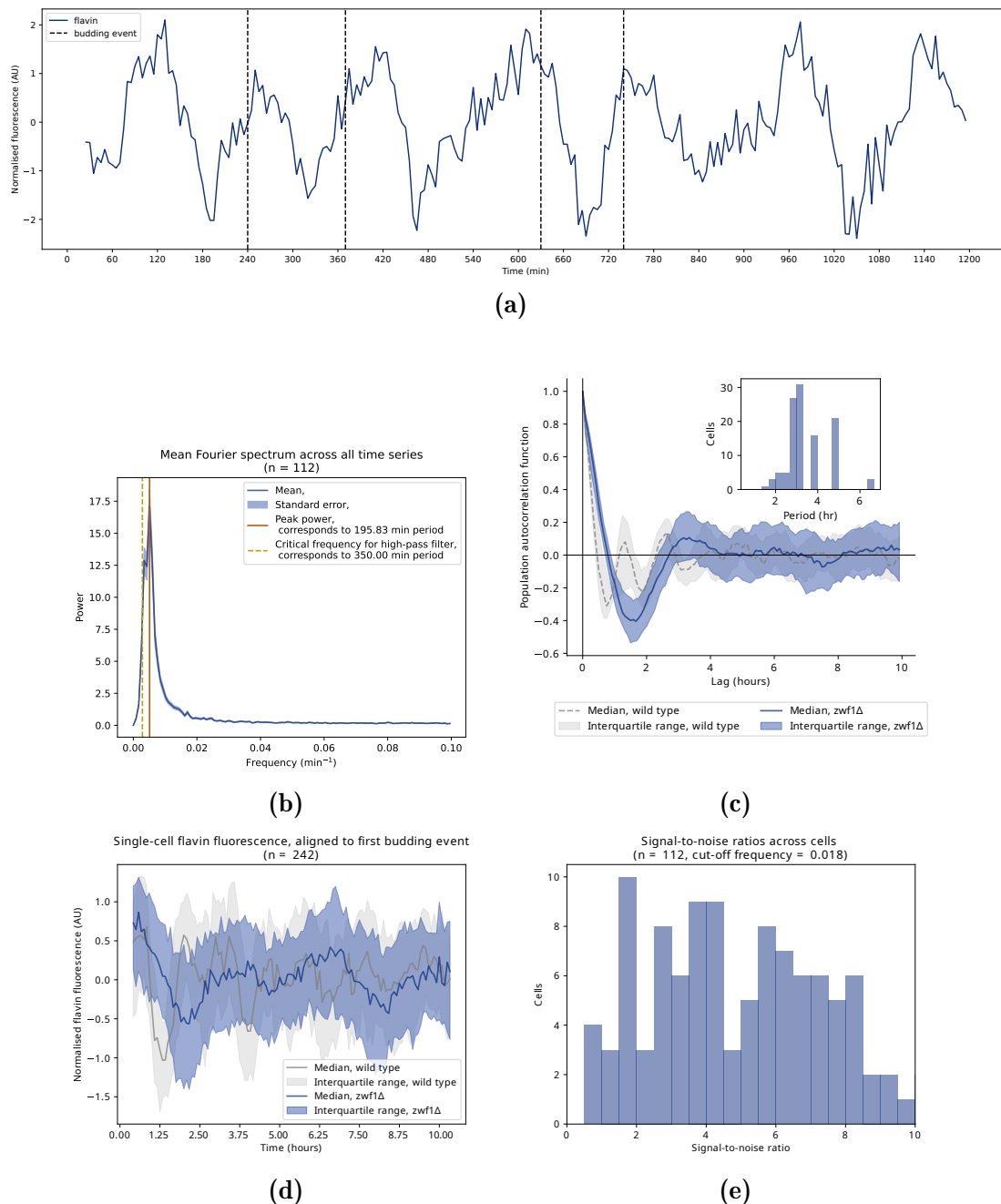


Figure 1.20: **(1.20a)** Flavin fluorescence (blue, solid lines) levels in a single, representative $\text{zwf1}\Delta$ cell. Vertical lines (black, dashed) indicate budding events. **(1.20b)** Mean Fourier spectrum of flavin fluorescence across cells. **(1.20c)** Median autocorrelation function of flavin fluorescence time series, along with (*inset*) the periods across cells as determined by the frequency with the greatest power in each signal's Fourier spectrum. **(1.20d)** Median flavin fluorescence signal across cells, aligned to first budding event. **(1.20e)** Distribution of signal-to-noise ratios of flavin signals from cells. Data are from $\text{zwf1}\Delta$ (BY4741) cells in 10 g L^{-1} glucose.

distribution of signal-to-noise ratios, while the reference BY4741 strain showed robust flavin oscillations of approximately 1.5 h. These results conflict with the results from the chemostat-based study (Tu et al., 2007) that suggested that metabolic cycles are abolished in this strain.

To investigate whether the *tsa1Δ tsa2Δ* strain shows metabolic oscillations of a different waveform in single-cell microfluidics, I used a *tsa1Δ tsa2Δ* strain with the BY4742 background. Chemostat-based studies suggest that in the *tsa1Δ tsa2Δ* strain, metabolic cycles are shorter and exhibit an M-shaped dissolved oscillation trace due to an additional dip of oxygen consumption in the reductive-charging phase (Causton et al., 2015). To be consistent with *zwf1Δ*, cells were pre-cultured and cultured in the same conditions, but with the appropriate supplements for the auxotrophy of BY4742.

Fig. 1.21 suggests that the metabolic cycles generated from the auxotrophic *tsa1Δ tsa2Δ* strain were not consistent, likely due to multiple periods. Specifically, the Fourier spectra (Fig. 1.21b) suggest that 2.45 h and 3.92 h oscillations were prominent in the population. These two prominent periods were obscured by the median fluorescence signal aligned by first budding event (Fig. 1.21d), which merely suggests that a 3 h oscillation was prominent in the population, and by the median autocorrelation function (Fig. 1.21c), which suggests that the oscillations were not at a consistent frequency across the population, in contrast to the BY4742 wild-type that showed robust 1.5 h oscillations. Fig. 1.21e additionally shows that the amplitudes and qualities of oscillations were retained, as evidenced by signal-to-noise ratios comparable to the FY4 strain cultured in pyruvate (Fig. 1.14b).

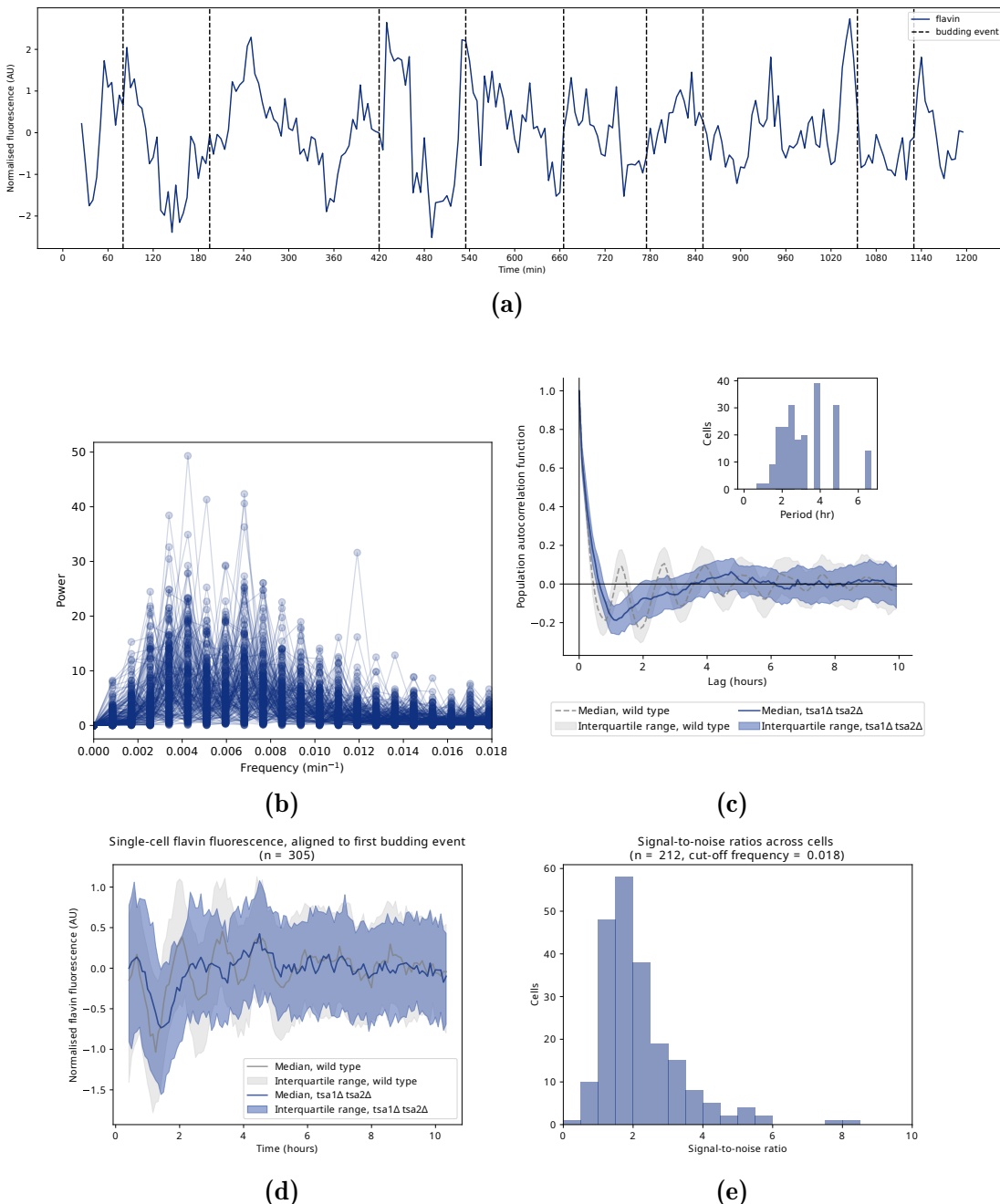


Figure 1.21: (1.21a) Flavin fluorescence (blue, solid lines) levels in a single, representative $\text{tsa1}\Delta \text{tsa2}\Delta$ cell. Vertical lines (black, dashed) indicate budding events. (1.21b) Overlaid Fourier spectra of flavin fluorescence across cells ($n = 212$). (1.21c) Median autocorrelation function of flavin fluorescence time series, along with (inset) the periods across cells as determined by the frequency with the greatest power in each signal's Fourier spectrum. (1.21d) Median flavin fluorescence signal across cells, aligned to first budding event. (1.21e) Distribution of signal-to-noise ratios of flavin signals from cells. Data are from $\text{tsa1}\Delta \text{tsa2}\Delta$ (BY4742) cells in 10 g L^{-1} glucose.

Taken together, there are striking discrepancies between the metabolic cycle observed as dissolved oxygen oscillations from the chemostat and the metabolic cycle observed as flavin autofluorescence oscillations in single-cell conditions in the *zwf1Δ* and *tsa1Δ tsa2Δ* deletion strains. These discrepancies warrant further explanation.

1.7 Discussion

1.7.1 Interpretation of results

This chapter confirms the presence of flavin-based single-cell metabolic cycles, and further confirm that they are autonomous and **may** gate the cell division cycle across nutrient and genetic perturbations.

Results suggest that yeast cells independently generate the metabolic cycle which locks the cell division cycle in-phase. This conclusion was supported by the observation that flavin cycles were asynchronous between cells and peaks coincide with bud formation. These observations were consistent with Papagiannakis et al. (2017) and Baumgartner et al. (2018).

Results in pyruvate additionally reveal that as the metabolic cycle lengthens, G₁ lengthens but S/M stays the same length, suggesting a model in which a specific phase of the metabolic cycle gates entry into the cell division cycle. Importantly, metabolic cycles still occurred even when cells did not divide. This holds true for one-off skipping of cell division and conditions in which cells pause cell division for long periods of time.

Results additionally show that the metabolic cycle and the cell division cycle can be decoupled, reinforcing the idea that the metabolic cycle is autonomous from other cellular oscillators. In particular, I observed that single-cell flavin oscillations could synchronise and reset phase in response to abrupt starvation, while the cell division cycle was paused. This observation also suggests that the metabolic cycle is individually generated across cells without the need of a diffusible metabolite as proposed by Krishna and Laxman (2018). The conclusion that the metabolic cycle is generated independently across cells is evidenced by the continued presence of metabolic cycles during starvation even though the cells were physically separated, with nutrient media perfused across them.

The distributions of flavin and mCherry signals during starvation provided some mechanistic basis for the coupling or decoupling between the two oscillators. This observation suggests that if starvation occurs before START, the cell remains in the G₁ phase. Otherwise, the cell proceeds through the cell division cycle until it pauses in the G₂ phase. Such observations strengthen the idea that the metabolic cycle independently gates the early (START) and the late (mitotic exit) phases of the cell division cycle (Özsezen et al., 2019). However, the biochemical mechanism by which the cell uses to reset the phase of its metabolic cycle remains unclear.

My observations confirm that cells adapt their metabolic cycle to nutrient conditions: the behaviour of the metabolic cycle changes when the cells are grown on low glucose or on pyruvate. A possible explanation is that nutrient conditions that favour respiration over fermentation — and thus slower growth rate — leads to slower YMCs.

My results

Results suggest discrepancies between chemostat and single-cell studies of the metabolic cycle, in particular, with regards to potassium-deficient conditions and the *zwf1Δ* and *tsa1Δ tsa2Δ* deletion strains. Such discrepancies warrant models to explain the observations.

I observed that metabolic cycles persist in potassium-deficient conditions, in contrast to O' Neill et al. (2020) which suggested that the oscillations disappear. The disappearance of dissolved oxygen cycles can alternatively be explained by a loss of synchrony in the population.

I also observed that *zwf1Δ* exhibited metabolic cycles, though with varying amplitudes. This contrasts Tu et al. (2007), which suggested that metabolic cycles in this strain were abolished To reconcile findings, a potential explanation is that cells lose synchrony or the ability to reset phase, while growth is still maintained. *ZWF1* codes for glucose-6-phosphate dehydrogenase, which catalyses the first step of the pentose phosphate pathway involving the reduction of NADP⁺ to produce NADPH, a key metabolite in the YMC (Nogae and Johnston, 1990). Thus, it is expected that the *zwf1Δ* deletion should affect a broad range of metabolic processes, including flavin oscillations, owing to the role of NAD(P)H redox in the function of the most abundant flavoproteins (Gudipati et al., 2014). However, some of the deleterious effects of *zwf1Δ* deletion may be compensated by *ALD6* and *IDP2* as they also catalyse reactions that produce NADPH (Minard and McAlister-Henn, 2005), therefore, explaining why growth is retained in the *zwf1Δ* strain.

Results additionally suggest that *tsa1Δ tsa2Δ* exhibits a range of metabolic cycle frequencies. This observation can be reconciled with the M-shaped dissolved oxygen cycles described by Causton et al. (2015) through a potential explanation: there are at least two substantial cell populations that each produce a different

frequencies of metabolic oscillations, and the changed M-shaped waveform is the sum of the effect of individual cells. *TSA1* and *TSA2* are paralogous genes that are involved in redox metabolism. Specifically, these genes code for peroxiredoxins as part of the peroxiredoxin-thioredoxin system, which functions to reduce intracellular reactive oxygen species (Wong et al., 2002). In addition, these genes have been suggested to be linked to the circadian rhythm, as evidenced by an approximately 24 h oscillation in oxidation patterns (Edgar et al., 2012). Therefore, deletion of these genes may lead to loss of regulation of timekeeping, leading to the different oscillation frequencies.

Taken together, the discrepancies between chemostat and single-cell studies highlight the role of sub-populations that cannot be captured in the chemostat, but possible in single-cell studies.

1.7.2 Study caveats and future directions

Characteristics of the single-cell metabolic cycle

Time series of NAD(P)H oscillations, especially if recorded alongside flavin in the same cells, would strengthen the evidence that flavin autofluorescence oscillations are equivalent to the single-cell metabolic oscillations described by previous microfluidics studies. Such data would also provide a novelty: two fluorophores that act as read-outs of the metabolic cycle have, to my knowledge, never been recorded from the same cell.

To explore the link between the components of flavin autofluorescence and cycling of storage lipids as a proposed biochemical mechanism of the metabolic cycle, the *fas1Δ* strain may be studied. *FAS1* codes for the most abundant flavoprotein, the beta subunit of fatty acid synthetase, which has a role in lipid metabolism

(Gudipati et al., 2014). The investigation may be strengthened with a rescue experiment using lipid sources such as glycerol trihexanoate or glycerol trioctanoate. This avenue of exploration may lead to additional insight on the biochemical basis of the yeast metabolic cycle, which is still poorly characterised.

To explore the conditions that make budding yeast cells reset their metabolic cycle phases, future experiments may include adding carbon sources in bulk, using the media-switching system of ALCATRAS. Such experiments could include acetate, acetaldehyde, or ethanol (Kuang et al., 2017; Krishna and Laxman, 2018). Insights from such experiments may lead to a broader understanding of the control of the sequence of events in the metabolic cycle.

Chemostat vs single-cell

Additional nutrient conditions can be used to address the discrepancies between the chemostat and single-cell microfluidics, namely, low glucose conditions and feast-and-famine conditions.

Low glucose conditions emulate conditions in the chemostat and may lead to long metabolic cycles, thus explaining why cycles with periods up to 14 h have been observed in chemostats. However, the glucose concentrations in chemostats are below the tolerance of measurement with current technologies, **we propose?** therefore the limiting concentration of 10 mg L^{-1} used in this chapter can be used. Experiments with deletion strains can then be performed under these low-glucose conditions to investigate whether such conditions lead to a closer equivalence between chemostat and single-cell studies.

Feast-and-famine conditions have been modelled in chemostat cultivation of yeast (Jones and Kompala, 1999). Further experiments can therefore use rapid media-switching in ALCATRAS to produce regular glucose pulsing. In this type of experiment, cells are fed with a glucose-limited medium for an amount of time, then switched on to a glucose-rich medium for a short period of time (approximately 10 min), and the cycle repeats. The interval between glucose pulses can be varied to investigate the effect of an external entraining mechanism on the system of coupled oscillators that defines the yeast metabolic cycle. This design would be similar to Charvin et al. (2009), which investigated the effect of intervals of glucose pulsing on the cell division and circadian cycles in budding yeast. A glucose pulsing experiment can thus also lead to a mathematical model of coupled oscillations in the yeast metabolic cycle.

Chapter 2

Methods

2.1 Strains and media

The *S. cerevisiae* strains used in this thesis are described in table 2.1.

The minimal medium described by (Verduyn et al., 1992) was used unless otherwise stated. This minimal medium does not contain riboflavin, thus minimising its effect on flavin autofluorescence imaging, and its composition is known and easily controlled. Specifically, the composition of the carbon source-limiting medium are described in tables 2.2–2.4, and the media pH was adjusted to 6.0 before use using potassium hydroxide, or sodium hydroxide for potassium-free media. For auxotrophic strains, supplements were added according to table 2.5. Then, a carbon source is added as appropriate to create the growth medium.

| Name | Background | Genotype | Origin | Notes |
|---------------|--------------|------------------------------------------|--------------------------------|------------------------------|
| FY4 | FY4 | - | EUROSCARF | Winston et al. (1995) |
| htb2::mCherry | FY4 | HTB2::mCherry | In-house, CRISPR | - |
| BY4741 | BY4741 | <i>MATa his3Δ1 leu2Δ0 met15Δ0 ura3Δ0</i> | EUROSCARF | Brachmann et al. (1998) |
| zwf1Δ | BY4741 | zwf1Δ::KAN | Edinburgh Genome Foundry | Yeast deletion collection |
| BY4742 | BY4742 | <i>MATa his3Δ1 leu2Δ0 lys2Δ0 ura3Δ0</i> | Bruce Morgan | Calabrese et al. (2019) |
| tsa1Δ tsa2Δ | BY4742 | tsa1Δ::natNT2 tsa2Δ::kanMX4 | Bruce Morgan | Calabrese et al. (2019) |
| CEN.PK113-7D | CEN.PK113-7D | - | Peter Kötter | Nijkamp et al. (2012) |

Table 2.1: Strains used in this thesis.

| Reagent | Concentration | Remarks |
|---------------------------------------------|------------------------|------------------------------|
| KH_2PO_4 | 3 g L^{-1} | |
| $\text{MgSO}_4 \cdot 7 \text{ H}_2\text{O}$ | 0.5 g L^{-1} | |
| $(\text{NH}_4)_2\text{SO}_4$ | 5 g L^{-1} | |
| Trace metals | 1 mL L^{-1} | See table 2.3 |
| Vitamins | 1 mL L^{-1} | See table 2.4. Add upon use. |
| Carbon source | variable | Add upon use. |

Table 2.2: Composition of base minimal medium. For potassium-free media, replace KH_2PO_4 with 2.65 g L^{-1} NaH_2PO_4 , which gives the same molarity.

| Reagent | Formula | Concentration [g L^{-1}] |
|-------------------------|-----------------------------------------------------------------------------------------|-------------------------------------|
| EDTA | $\text{C}_{10}\text{H}_{14}\text{N}_2\text{Na}_2\text{O}_8 \cdot 2 \text{ H}_2\text{O}$ | 15.00 |
| Zinc sulfate | $\text{ZnSO}_4 \cdot 7 \text{ H}_2\text{O}$ | 4.50 |
| Manganese (II) chloride | $\text{MnCl}_2 \cdot 2 \text{ H}_2\text{O}$ | 0.84 |
| Cobalt (II) chloride | $\text{CoCl}_2 \cdot 6 \text{ H}_2\text{O}$ | 0.30 |
| Copper (II) sulfate | $\text{CuSO}_4 \cdot 5 \text{ H}_2\text{O}$ | 0.30 |
| Sodium molybdate | $\text{Na}_2\text{MoO}_4 \cdot 2 \text{ H}_2\text{O}$ | 0.40 |
| Calcium chloride | $\text{CaCl}_2 \cdot 2 \text{ H}_2\text{O}$ | 4.50 |
| Iron (II) sulfate | $\text{FeSO}_4 \cdot 7 \text{ H}_2\text{O}$ | 3.00 |
| Boric acid | H_3BO_3 | 1.00 |
| Potassium iodide | KI | 0.10 |

Table 2.3: Composition of trace metal mix for minimal media described in table 2.2.

| Reagent | Formula | Concentration [g L ⁻¹] |
|---------------------------------|------------------------------------------------------------------|------------------------------------|
| D-(+)-biotin | C ₁₀ H ₁₆ N ₂ O ₃ S | 0.05 |
| D-pantothenic acid calcium salt | Ca(C ₉ H ₁₆ NO ₅) ₂ | 1.00 |
| Nicotinic acid | C ₆ H ₅ NO ₂ | 1.00 |
| <i>myo</i> -Inositol | C ₆ H ₁₂ O ₆ | 25.00 |
| Thiamine chloride hydrochloride | C ₁₂ H ₁₅ ClN ₄ OS · HCl | 1.00 |
| Pyridoxal hydrochloride | C ₈ H ₁₂ ClNO ₃ | 1.00 |
| 4-aminobenzoic acid | C ₇ H ₇ NO ₂ | 0.20 |

Table 2.4: Composition of vitamin mix for minimal media described in table 2.2.

| Reagent | Concentration [mg L ⁻¹] |
|------------|-------------------------------------|
| histidine | 125 |
| leucine | 500 |
| tryptophan | 75 |
| methionine | 100 |
| uracil | 150 |

Table 2.5: Supplements to minimal media for BY4741-background auxotrophic strains, compositions derived from Pronk (2002). For BY4742-background strains, replace methionine with 100 mg L⁻¹ lysine-HCl.

2.2 Single-cell microfluidics

Cells were grown from colonies on solid agar in a liquid culture composed of minimal media formulation appropriate for the experiment, supplements appropriate for the strain's auxotrophy, and a carbon source (glucose or pyruvate) appropriate for the experiment (see section 2.1). The cells were incubated at 30 °C for 14 h (overnight) if the carbon source is glucose or 48 h if the carbon source is pyruvate. Subsequently, the cells were diluted so that the resulting culture had an OD₆₀₀ of 0.10–0.20, and were then incubated for a further 4 h.

ALCATRAS microfluidics (Crane et al., 2014) devices were then prepared and for an experiment, one device's multiple chambers were filled with growth media supplemented with 0.05% w/v bovine serum albumin. Cells were then loaded into the ALCATRAS chambers — different chambers can house cells from different

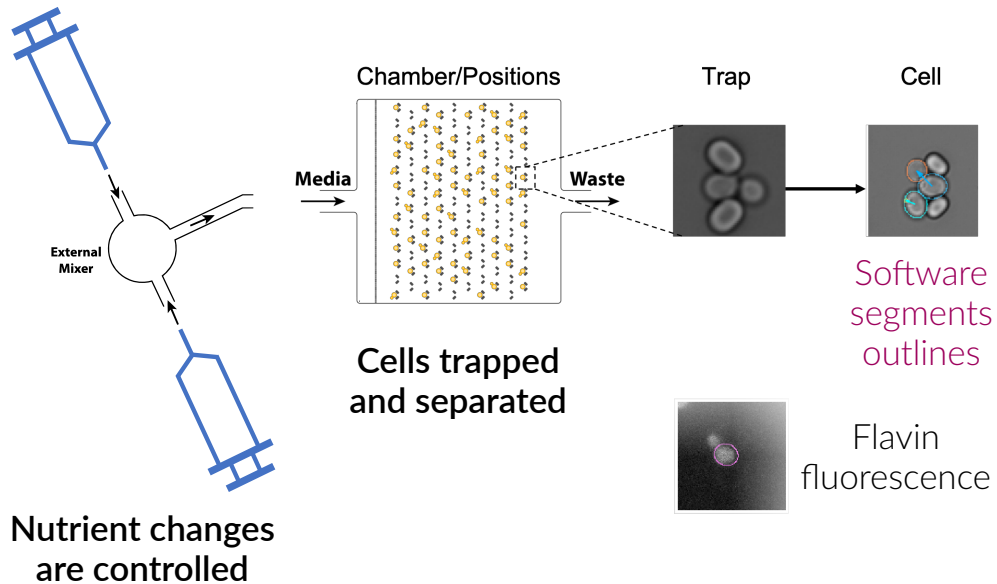


Figure 2.1: Overview of single-cell microfluidics set-up using the ALCATRAS system. Cells are loaded into chambers within devices, where they are trapped and separated (centre). The media composition the cells experience are controlled with syringe pumps (left). Brightfield and fluorescent images are taken at regular intervals, and then processed using *aliby* to provide time series of fluorescence intensity changes for each parent cell. cite Alan's thesis (?)

strains (figure 2.1). Syringe pumps containing media were programmed to produce a constant flow of $4 \mu\text{L h}^{-1}$ into the chambers. As a consequence, parent cells are held in place within traps, while progeny cells flow out of traps into the outflow after they bud. There are two syringes that can contain different media, and in experiments that require different nutrient conditions at different times, the ALCATRAS system is programmed to switch between the two syringes. The cells and ALCATRAS chambers were located in an incubation chamber (Oko-labs) that was maintained at 30°C .

Microscopy was performed using a $60 \times 1.4 \text{ NA}$ oil immersion objective (Nikon), and the Nikon Perfect Focus System was used to ensure consistent focus. X-Y spatial positions were defined for each chamber to maximise spatial coverage of the chamber while ensuring that the microscope takes less time to move positions and capture images than the interval period. Images were taken every 5 min, and image

acquisition duration varied for each experiment. Brightfield and flavin images were captured in all strains and mCherry images were additionally captured for the HTB2::mCherry strain. Five z-slices were taken for brightfield images, with a spacing of 0.6 µm between slices. Fluorescence imaging was performed with an OptoLED light source (Cain Research), and LED voltage was optimised for maximum signal intensity without LED cut-off prior to experiments. For flavin imaging, the excitation filter was set to 430/24 (418 nm to 442 nm), the emission filter was set to 535/30 (520 nm to 550 nm), and the exposure time was 60 ms. One z-slice was taken for each flavin image in each position. For mCherry imaging, the excitation filter was set to 555 nm to 590 nm), the emission filter was set to 632/60 (602 nm to 682 nm) and the exposure time was 100 ms. Five z-slices were taken for mCherry images, with a spacing of 0.6 µm between slices.

might explain
the reduction in
growth rate

2.3 Segmentation, extraction, post-processing

I used *aliby* (Muñoz González, 2023), an end-to-end Python-based software package developed for time-lapse microscopy, to process the microscope images in order to obtain flavin and mCherry time series for further analysis.

aliby tracks tiles that correspond to a trap across time-lapse images to account for expected spatial drifting in the microscope. It then uses *BABY* (Pietsch et al., 2023) to segment the images of traps to identify the outlines of cells and to track cells from one time point to another, creating a lineage of cells. *aliby* then overlays the cell outlines onto the fluorescent (flavin and mCherry) images to extract fluorescence intensity, and assigns a fluorescence value to each cell at each time point based on the mean intensity of pixels within the cell's outline. The background fluorescence is also computed, based on the pixel intensity outside cell outlines, and is then subtracted from the cell fluorescence. Flavin fluorescence

thus represents the oxidation of flavins throughout the yeast metabolic cycle (see section ??), and mCherry fluorescence thus represents the amount of histone proteins as a proxy for cell division cycle progression (Garmendia-Torres et al., 2018).

Bibliography

- Bagamery, L. E., Q. A. Justman, E. C. Garner and A. W. Murray (2020). “A Putative Bet-Hedging Strategy Buffers Budding Yeast against Environmental Instability”. In: *Current Biology*.
- Baumgartner, B. L., R. O’Laughlin, M. Jin, L. S. Tsimring, N. Hao and J. Hasty (2018). “Flavin-Based Metabolic Cycles Are Integral Features of Growth and Division in Single Yeast Cells”. In: *Scientific Reports* 8.1, pp. 1–10.
- Brachmann, C. B., A. Davies, G. J. Cost, E. Caputo, J. Li, P. Hieter and J. D. Boeke (1998). “Designer Deletion Strains Derived from *Saccharomyces Cerevisiae* S288C: A Useful Set of Strains and Plasmids for PCR-mediated Gene Disruption and Other Applications”. In: *Yeast* 14.2, pp. 115–132.
- Calabrese, G., E. Peker, P. S. Amponsah, M. N. Hoehne, T. Riemer, M. Mai, G. P. Bienert, M. Deponte, B. Morgan and J. Riemer (2019). “Hyperoxidation of Mitochondrial Peroxiredoxin Limits H₂O₂-induced Cell Death in Yeast”. In: *The EMBO Journal* 38.18, e101552.
- Causton, H. C., K. A. Feeney, C. A. Ziegler and J. S. O’Neill (2015). “Metabolic Cycles in Yeast Share Features Conserved among Circadian Rhythms”. In: *Current Biology* 25.8, pp. 1056–1062.
- Charvin, G., F. R. Cross and E. D. Siggia (2009). “Forced Periodic Expression of G1 Cyclins Phase-Locks the Budding Yeast Cell Cycle”. In: *Proceedings of the National Academy of Sciences* 106.16, pp. 6632–6637.

- Crane, M. M., I. B. N. Clark, E. Bakker, S. Smith and P. S. Swain (2014). “A Microfluidic System for Studying Ageing and Dynamic Single-Cell Responses in Budding Yeast”. In: *PLOS ONE* 9.6, e100042.
- Edgar, R. S., E. W. Green, Y. Zhao, G. van Ooijen, M. Olmedo, X. Qin, Y. Xu, M. Pan, U. K. Valekunja, K. A. Feeney, E. S. Maywood, M. H. Hastings, N. S. Baliga, M. Merrow, A. J. Millar, C. H. Johnson, C. P. Kyriacou, J. S. O'Neill and A. B. Reddy (2012). “Peroxiredoxins Are Conserved Markers of Circadian Rhythms”. In: *Nature* 485.7399, pp. 459–464.
- Garmendia-Torres, C., O. Tassy, A. Matifas, N. Molina and G. Charvin (2018). “Multiple Inputs Ensure Yeast Cell Size Homeostasis during Cell Cycle Progression”. In: *eLife* 7. Ed. by A. Musacchio, e34025.
- Gudipati, V., K. Koch, W.-D. Lienhart and P. Macheroux (2014). “The Flavoproteome of the Yeast *Saccharomyces Cerevisiae*”. In: *Biochimica et Biophysica Acta (BBA) - Proteins and Proteomics* 1844.3, pp. 535–544.
- Herskowitz, I. (1988). “Life Cycle of the Budding Yeast *Saccharomyces Cerevisiae*”. In: *Microbiological Reviews* 52.4, pp. 536–553.
- Jones, K. D. and D. S. Kompala (1999). “Cybernetic Model of the Growth Dynamics of *Saccharomyces Cerevisiae* in Batch and Continuous Cultures”. In: *Journal of Biotechnology. Modelling in Biochemical Engineering* 71.1, pp. 105–131.
- Krishna, S. and S. Laxman (2018). “A Minimal “Push–Pull” Bistability Model Explains Oscillations between Quiescent and Proliferative Cell States”. In: *Molecular Biology of the Cell* 29.19, pp. 2243–2258.
- Kuang, Z., S. Pinglay, H. Ji and J. D. Boeke (2017). “Msn2/4 Regulate Expression of Glycolytic Enzymes and Control Transition from Quiescence to Growth”. In: *eLife* 6. Ed. by N. Barkai, e29938.

- Minard, K. I. and L. McAlister-Henn (2005). “Sources of NADPH in Yeast Vary with Carbon Source*”. In: *Journal of Biological Chemistry* 280.48, pp. 39890–39896.
- Muñoz González, A. F. (2023). “Phenotyping Single Cells of *Saccharomyces Cerevisiae* Using an End-to-End Analysis of High-Content Time-Lapse Microscopy”. PhD thesis. University of Edinburgh.
- Murray, D. B., K. Haynes and M. Tomita (2011). “Redox Regulation in Respiring *Saccharomyces Cerevisiae*”. In: *Biochimica et Biophysica Acta (BBA) - General Subjects*. Systems Biology of Microorganisms 1810.10, pp. 945–958.
- Nijkamp, J. F., M. van den Broek, E. Datema, S. de Kok, L. Bosman, M. A. Luttik, P. Daran-Lapujade, W. Vongsangnak, J. Nielsen, W. H. Heijne, P. Klaassen, C. J. Paddon, D. Platt, P. Kötter, R. C. van Ham, M. J. Reinders, J. T. Pronk, D. de Ridder and J.-M. Daran (2012). “De Novo Sequencing, Assembly and Analysis of the Genome of the Laboratory Strain *Saccharomyces Cerevisiae* CEN.PK113-7D, a Model for Modern Industrial Biotechnology”. In: *Microbial Cell Factories* 11.1, p. 36.
- Nogae, I. and M. Johnston (1990). “Isolation and Characterization of the ZWF1 Gene of *Saccharomyces Cerevisiae*, Encoding Glucose-6-Phosphate Dehydrogenase”. In: *Gene* 96.2, pp. 161–169.
- O’Neill, J. S., N. P. Hoyle, J. B. Robertson, R. S. Edgar, A. D. Beale, S. Y. Peak-Chew, J. Day, A. S. H. Costa, C. Frezza and H. C. Causton (2020). “Eukaryotic Cell Biology Is Temporally Coordinated to Support the Energetic Demands of Protein Homeostasis”. In: *Nature Communications* 11.1, p. 4706.
- Özsezen, S., A. Papagiannakis, H. Chen, B. Niebel, A. Milias-Argeitis and M. Heinemann (2019). “Inference of the High-Level Interaction Topology between the Metabolic and Cell-Cycle Oscillators from Single-Cell Dynamics”. In: *Cell Systems*.

- Papagiannakis, A., B. Niebel, E. C. Wit and M. Heinemann (2017). “Autonomous Metabolic Oscillations Robustly Gate the Early and Late Cell Cycle”. In: *Molecular Cell* 65.2, pp. 285–295.
- Pietsch, J. M., A. F. Munoz, D.-Y. A. Adjavon, I. Farquhar, I. B. Clark and P. S. Swain (2023). “Determining Growth Rates from Bright-Field Images of Budding Cells through Identifying Overlaps”. In: *eLife* 12. Ed. by A. M. Moses, e79812.
- Pronk, J. T. (2002). “Auxotrophic Yeast Strains in Fundamental and Applied Research”. In: *Applied and Environmental Microbiology* 68.5, pp. 2095–2100.
- Siano, S. A. and R. Mutharasan (1989). “NADH and Flavin Fluorescence Responses of Starved Yeast Cultures to Substrate Additions”. In: *Biotechnology and Bioengineering* 34.5, pp. 660–670.
- Tu, B. P., R. E. Mohler, J. C. Liu, K. M. Dombek, E. T. Young, R. E. Synovec and S. L. McKnight (2007). “Cyclic Changes in Metabolic State during the Life of a Yeast Cell”. In: *Proceedings of the National Academy of Sciences* 104.43, pp. 16886–16891.
- Verduyn, C., E. Postma, W. A. Scheffers and J. P. V. Dijken (1992). “Effect of Benzoic Acid on Metabolic Fluxes in Yeasts: A Continuous-Culture Study on the Regulation of Respiration and Alcoholic Fermentation”. In: *Yeast* 8.7, pp. 501–517.
- Winston, F., C. Dollard and S. L. Ricupero-Hovasse (1995). “Construction of a Set of Convenient *Saccharomyces Cerevisiae* Strains That Are Isogenic to S288C”. In: *Yeast* 11.1, pp. 53–55.
- Wong, C.-M., Y. Zhou, R. W. M. Ng, H.-f. Kung and D.-Y. Jin (2002). “Cooperation of Yeast Peroxiredoxins Tsa1p and Tsa2p in the Cellular Defense against Oxidative and Nitrosative Stress *”. In: *Journal of Biological Chemistry* 277.7, pp. 5385–5394.